Acta Oceanol. Sin., 2019, Vol. 38, No. 3, P. 114–123
https://doi.org/10.1007/s13131-019-1404-8
http://www.hyxb.org.cn
E-mail: hyxbe@263.net

Undrained shear strength evaluation for hydrate-bearing sediment overlying strata in the Shenhu area, northern South China Sea

Yanlong Li[1, 2, 3], Gaowei Hu[1, 2, 3], Nengyou Wu[1, 2, 3]*, Changling Liu[1, 2, 3], Qiang Chen[1, 2, 3], Chen'an Li[1, 3, 4]

[1] Key Laboratory of Gas Hydrate, Ministry of Natural Resources, Qingdao 266071, China

[2] Laboratory for Marine Mineral Resource, Pilot National Laboratory for Marine Science and Technology (Qingdao), Qingdao 266071, China

[3] Qingdao Institute of Marine Geology, China Geological Survey, Qingdao 266071, China

[4] College of Information and Control Engineering, China University of Petroleum, Qingdao 266580, China

Received 10 January 2018; accepted 27 February 2018

Abstract

The undrained shear strength of shallow strata is a critical parameter for safety design in deep-water operations. *In situ* piezocone penetration tests (CPTU) and laboratory experiments are performed at Site W18-19 in the Shenhu area, northern South China Sea, where China's first marine hydrate exploitation operation is due to be located. The validation of the undrained shear strength prediction model based on CPTU parameters. Different laboratory tests, including pocket penetrometer, torvane, miniature vane and unconsolidated undrained triaxial tests, are employed to solve empirical cone coefficients by statistical and mathematical methods. Finally, an optimized model is proposed to describe the longitudinal distribution of undrained shear strength in calcareous clay strata in the Shenhu area. Research results reveal that average empirical cone coefficients based on total cone resistance, effective resistance, and excess-pore pressure are 13.8, 4.2 and 14.4, respectively. The undrained shear strength prediction model shows a good fit with the laboratory results only within specific intervals based on their compaction degree and gas-bearing conditions. The optimized prediction model in piecewise function format can be used to describe the longitudinal distribution of the undrained shear strength for calcareous clay within all depth intervals from the mud-line to the upper boundary of hydrate-bearing sediments (HBS). The optimized prediction result indicates that the effective cone resistance model is suitable for very soft to firm calcareous clays, the excess-pore pressure model can depict the undrained shear strength for firm to very stiff but gas-free clays, while the total cone resistance model is advantageous for evaluating the undrained shear strength for very stiff and gassy clays. The optimized model in piecewise function format can considerably improve the adaptability of empirical models for calcareous clay in the Shenhu area. These results are significant for safety evaluations of proposed hydrate exploitation projects.

Key words: piezocone penetration test, hydrate exploitation test, undrained shear strength, calcareous clay, Shenhu area, South China Sea

Citation: Li Yanlong, Hu Gaowei, Wu Nengyou, Liu Changling, Chen Qiang, Li Chen'an. 2019. Undrained shear strength evaluation for hydrate-bearing sediment overlying strata in the Shenhu area, northern South China Sea. Acta Oceanologica Sinica, 38(3): 114–123, doi: 10.1007/s13131-019-1404-8

1 Introduction

Natural gas hydrate (NGH) is a caged crystalline solid formed from water and natural gas molecules. It is widely occurring in permafrost and the seabed at continental margins. The amount of the NGH hosted in continental margin sea beds is twice that hosted in permafrost (Kvenvolden, 1998; Wu et al., 2011). In 2007 and 2015, offshore drilling projects operated by the China Geology Survey (CGS) suggested that a large amount of the NGH (more than 1 500×10^8 m^3 natural gas equivalent) exists in the Shenhu area of the northern South China Sea (Wu et al., 2010; Yang et al., 2015; Liu et al., 2017; Wang et al., 2017). Because the NGH in this area is buried in clayey silt sediments, the geo-technical characteristics of overlying hydrate-bearing sediments (HBS) plays a crucial role in safe and effective gas production from the HBS strata (Han et al., 2015). Specifically, the undrained shear strength of shallow strata is vital for both deep-water jetting and wellhead stability analysis during the entire process of hydrate exploitation (Li et al., 2016a, b).

Laboratory experiments and *in situ* tests are popular ways to obtain undrained shearing strength (S_u) (Chung et al., 2006). However, because of limitations related to both sample quantity and quality, results from laboratory experiments can rarely represent the longitudinal distribution of the undrained shear strength in all depth intervals. *In situ* piezocone penetration tests

Foundation item: The National Natural Science Foundation of China under contract No. 41606078; the Taishan Scholar Special Experts Project under contract No. ts201712079; the National Key Research and Development Plan under contract No. 2017YFC0307600; the Open Fund of Qingdao National Laboratory for Marine Science and Technology of China under contract Nos QNLM2016ORP0203 and QNLM2016ORP0207.

*Corresponding author, E-mail: wuny@ms.giec.ac.cn

(CPTU) record cone resistance, sleeve friction, and pore pressure continually throughout the probing process; thus, a series of continuous and undisturbed undrained shear strength values can be predicted using theoretical methods or empirical/semi-empirical equations (Konrad and Law, 2015; Ching and Phoon, 2012). Because the CPTU probing process is too complicated to be modeled accurately, all theoretical methods are based on some assumptions and simplifications. These assumptions restrict the applications of theoretical methods in simulations of soil anisotropy, soil sensitivity, and soil geological ages under different stress history conditions (Ma et al., 2014; Ji et al., 2016). Empirical/semi-empirical equations provide a simple way to estimate the undrained shear strength using CPTU results, but empirical cone coefficients are always obtained by mathematical statistics of the test results from a given region and are not applicable to other areas. Research has shown a lack of studies related to CPTU analysis in the Shenhu area, northern South China Sea, where China's first marine NGH exploitation is to be implemented.

Fugro's WISON® (EP) system is used for CPTU analysis in NGH overlying strata in the Shenhu area. In this study, CPTU test parameters related to the undrained shear strength calculation are analyzed and empirical prediction models based on the CPTU tests are summarized. Methods for validating the relationships between CPTU data and different laboratory test results are provided, which mainly include pocket penetrometer, torvane, miniature vane and unconsolidated undrained triaxial tests. The cone coefficients for the undrained shear strength evaluation based on different empirical methods are fitted and the longitudinal distribution of the undrained shear strength in the overlying HBS strata is analyzed. Finally, an optimized S_u prediction model in piecewise function format is proposed according to the fitting degree between predicted and laboratory measured results.

2 Empirical methods to estimate the undrained shear strength via CPTU results

As described above, theoretical modeling and empirical equations are two general methods for estimating the undrained shear strength via CPTU test results. Theoretical modeling provides the basis for establishing the empirical equations (Liu et al., 2013), which are the direct reflection of theoretical models and easier for field engineers to adopt. Therefore, empirical methods are the first choice for estimating the undrained shear strength via CPTU test results.

Briefly, empirical methods involve a series of statistical equations that reflect some of the internal relationships between the undrained shear strength and CPTU parameters. The three most popular empirical equations are summarized in Eqs (1) to (3), which are based on the total cone resistance, effective cone resistance, and excess-pore pressure, respectively (Lunne et al., 1987; Senneset et al., 1982; Tong et al., 2011).

$$S_{u,1} = \frac{q_t - \sigma_{v0}}{N_{kt}}, \tag{1}$$

$$S_{u,2} = \frac{q_t - u_2}{N_{ke}}, \tag{2}$$

$$S_{u,3} = \frac{u_2 - u_0}{N_{\Delta u}}, \tag{3}$$

where $S_{u,1}$, $S_{u,2}$ and $S_{u,3}$ represent S_u values based on the total cone resistance (kPa), effective cone resistance (kPa), and excess-pore pressure (kPa), respectively; q_t is the calibrated total cone resistance (kPa); σ_{vo} is total overburden stress (kPa); u_2 is pore pressure obtained by the WISON® (EP) system (kPa); u_0 is the hydrostatic pressure (kPa); and N_{kt}, N_{ke} and $N_{\Delta u}$ represent dimensionless empirical cone coefficients based on the total cone resistance, effective cone resistance, and excess-pore pressure, respectively.

Some previous studies have predicted the empirical cone coefficients based on mathematics and statistics. Typical research results are listed in Table 1, indicating that the average values of cone coefficients range from 8 to 24 for N_{kt}, 8.6 to 12 for N_{ke}, and 4 to 10 for $N_{\Delta u}$. It should be noted that all empirical cone coefficients listed in Table 1 are based on a specific test region and soil type. Large differences exist among empirical cone coefficients in different study areas, even for the same soil type. Furthermore, these previous studies rarely focused on calcareous clayey silt, which is common throughout the Shenhu area. Thus, the results in Table 1 provide only general guidelines but cannot be used to quantitatively calculate accurate longitudinal distributions of the undrained shear strength for calcareous clay in the

Table 1. Typical empirical cone coefficients

Coefficients	Value	Test region	Soil type	References
N_{kt}	8–16	North Sea and on shore, Norway	plastic clay	Aas et al. (1986)
N_{kt}	13.9	New Orleans, USA	high plasticity fat clay	Wei et al. (2010)
N_{kt}	16.3/19.6	Suzhou metro site, China	clay / silty clay	Yang et al. (2016)
N_{kt}	15	Shanghai, China	marine soft soil	
N_{ke}	8.62	Ningbo, China	clayey soil	Li et al. (2016c)
N_{kt}	16–18	South bank of Changjiang River, Jurong, China	silty sand	An et al. (2009)
N_{ke}	9–12			
$N_{\Delta u}$	4–7			
N_{kt}	16.5	Jiangsu Lixia River, China	lagoonal clay	Cai et al. (2016)
N_{kt}	$0.285I_p$+7.6	Indiana, USA	clayey soils	Shin and Kim (2011)
N_{kt}	10.4–13.2	Burswood, Australia	marine clay soil	Low and Randolph (2010)
N_{kt}	19–24	South Pars field, Iran	marine clay	Ebrahimian et al. (2012)
$N_{\Delta u}$	4–10	North Sea	clay	Lunne et al. (1987)
$N_{\Delta u}$	7–9	Canada	clay	La et al. (1990)
$N_{\Delta u}$	4–9	Busan Port, Korea	plastic clay	Hong et al. (2010)

Note: I_p represents plasticity index of soil.

Shenhu area.

3 Geological operation and coefficient determination

3.1 *Test results and basic soil characteristics*

Both CPTU tests and the geological coring operation were conducted at Site W18-19, where China's first marine NGH exploitation test has been proposed. The sea water depth of the operation site is approximately 1 270 m and the proposed operation depth is 140 meters below sea floor (mbsf), which is the upper boundary of the HBS strata. CPTU analysis was conducted using Fugro's WISON® EP System. The geometric sizes of the probe were as follows: 10 cm^2 base area, 60° cone, and a 150 cm^2 cylindrical sleeve (Hu et al., 2017). The filter element for a pore pressure measurement was located on the shoulder of the cone tip. The penetration rate during CPTU analysis was maintained at (20±5) mm/s.

According to Eqs (1)–(3), the calibrated total cone resistance (q_t) and pore pressure (u_2) are two crucial PCTU parameters that directly relate to the undrained shear strength estimation (Fig. 1). Figure 1 illustrates that both q_t and u_2 exhibit relatively consistent linear variation characteristics with an increase of depth below the seafloor, which indicates the same soil type deposition in the overlying HBS strata. The fluctuation of the CPTU curves is caused by small interlayers or penetration disturbances. An increase of the CPTU parameters indicates an increase in compaction degree with depth below the seafloor (Młynarek et al., 2012). This has been confirmed by a geological coring operation in an adjacent well. In the overlying strata, very soft calcareous clay, soft calcareous clay, firm calcareous clay, generally stiff calcareous clay, and very stiff calcareous clay were observed from top to bottom. This finding indicates that, for the same undrained shear strength prediction model (as shown in Eqs (1), (2) or (3), we can use unified cone factors to predict the vertical distribution of the undrained shear strength for the entire depth interval of the Shenhu area in the northern South China Sea.

Along with q_t and u_2, the total overburden stress (σ_{vo}) and the hydrostatic pressure (u_0) are two crucial parameters for the undrained shear strength estimation using the CPTU results, as shown in Eqs (1)–(3). Parameter σ_{vo} can be derived from the integral of soil wet specific gravity:

$$\sigma_{v0} = \int_0^H \gamma \mathrm{d}h, \tag{4}$$

where H is the target calculation depth (mbsf); and γ represents the wet specific gravity of soil obtained from the geological coring operation (kN/m^3). Parameter u_0 can be calculated using Eq. (5).

$$u_2 = \rho_w g H, \tag{5}$$

where ρ_w represents the density of pore water (g/cm^3); and g represents the gravitational acceleration (g=9.8 m/s^2). Finally, the distribution of σ_{vo} and u_0 in the tested depths of overlying strata is shown in Fig. 2.

3.2 *Determination of cone factors*

The undrained shear strength of soil varies according to failure mode, stress anisotropy, strain rate, and stress history. The undrained shear strength values obtained from different laboratory methods or *in situ* tests always exhibit differences. Therefore, the corresponding cone factors based on different laboratory experimental methods will also differ, and the detailed laboratory experimental method should be declared when calculating cone factors using mathematical and statistical methods.

The pocket penetrometer, torvane, miniature vane, and unconsolidated undrained triaxial tests are considered major tools for testing cohesive samples in the field, and are always used during sample classification in the laboratory. In order to establish the relationships between CPTU parameters and the undrained shear strength values, these tests were performed for samples acquired from a geological coring operation in an adjacent well. The following sections describe the method for predicting the empirical cone coefficients for empirical equations based on the

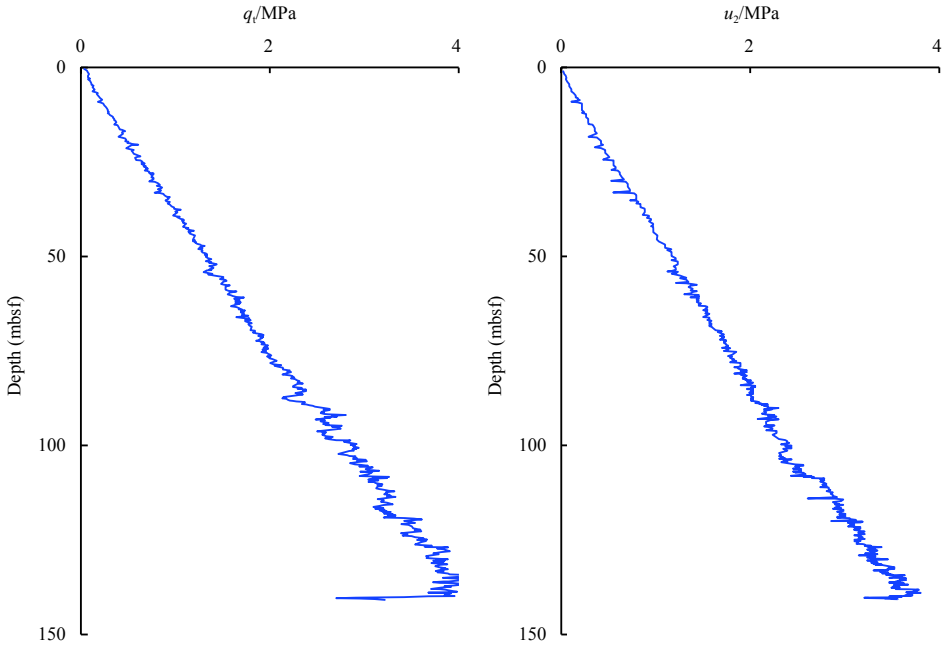

Fig. 1. q_t and u_2 distribution with depth below the seafloor.

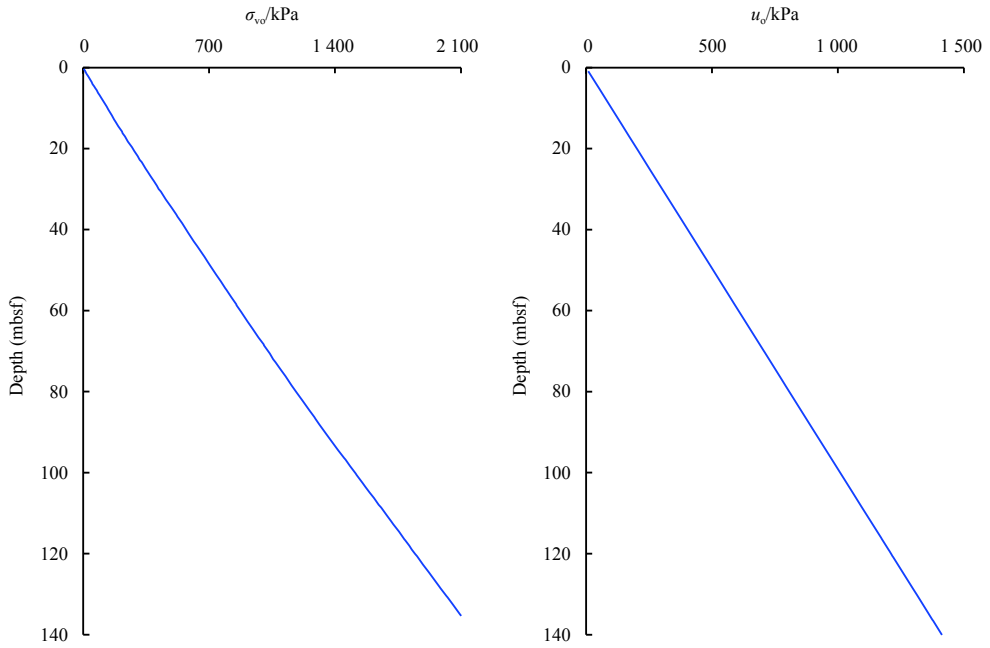

Fig. 2. σ_{vo} and $u_0$distribution with depth below the seafloor.

total cone resistance, the effective cone resistance, and the excess-pore pressure, respectively.

Because the distance between the CPTU test site and the coring well was small (within 10 m), if the depth value of the CPTU parameters equals that of the coring sample, we can assume that the CPTU parameters and the samples are in one-to-one correspondence; thus, the undrained shear strength values of a sample obtained by the laboratory experiments correspond to the CPTU parameters obtained from the same depth in the sample.

Thus, according to Eq. (1), we plot laboratory obtained undrained shear strength values as the *X*-axis and CPTU test "q_t–σ_{vo}" values as the *Y*-axis and establish a rectangular coordinate system. Then, scatter plots are obtained for each laboratory experimental method and the slope of a simple linear approximation of these scattered points through the origin equals N_{kt}, as shown in Eq. (1). Hence, the four types of laboratory experiments were used to calculate the empirical coefficients, resulting in four scatter plots and corresponding N_{kt} values, as shown in Fig. 3. $N_{kt, PP}$, $N_{kt, LV}$, $N_{kt, TV}$ and $N_{kt, UU}$ represent N_{kt} for calcareous clay strata based on the pocket penetrometer, torvane, miniature vane, and unconsolidated undrained triaxial tests, respectively. The total cone resistance coefficients obtained from Fig. 3 are: $N_{kt, PP}$=17.1, $N_{kt, TV}$=15.2, $N_{kt, LV}$=11.6, and $N_{kt, UU}$=11.1.

The calculation method for the effective cone resistance coefficient is similar to that for the total cone resistance coefficient. Laboratory-derived undrained shear strength values and CPTU

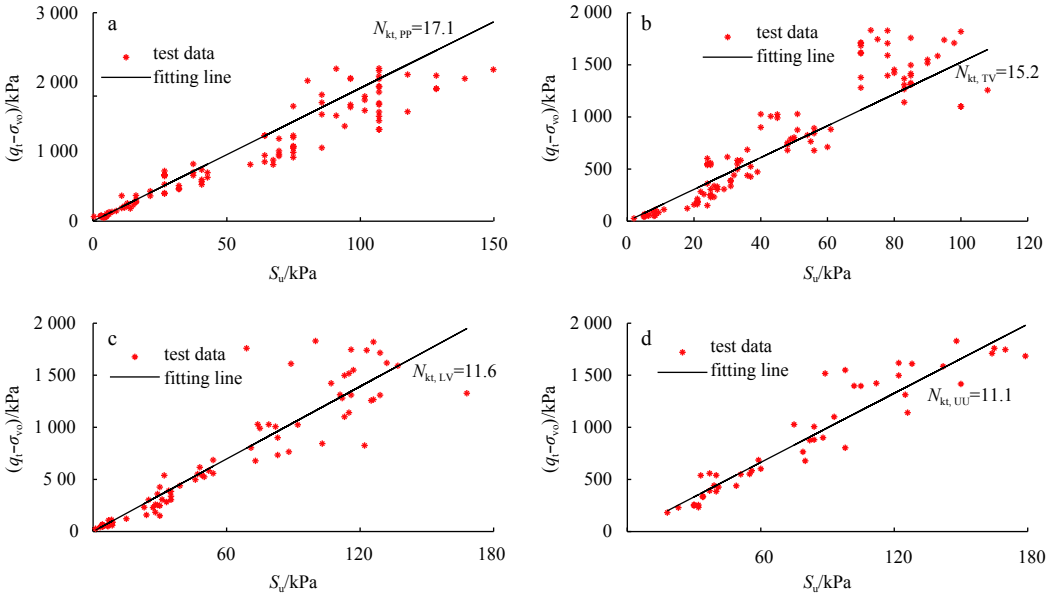

Fig. 3. Variations of q_t–σ_{vo} versus the undrained shear strength determined by pocket penetrometer (a), torvane (b), miniature vane (c), and UU triaxial tests (d).

test "q_t-u_2" values are plotted on the X-axis and Y-axis, respectively, to establish coordinate systems, resulting in scatter plots for each laboratory method. The slope of simple linear approximations to these scattered points through the origin equals N_{ke}. In Fig. 4, $N_{ke,\,PP}$, $N_{ke,\,LV}$, $N_{ke,\,TV}$ and $N_{ke,\,UU}$ represent N_{ke} for calcareous clay strata based on pocket penetrometer, torvane, miniature vane, and unconsolidated undrained triaxial tests, respectively. N_{ke} values obtained from Fig. 4 are $N_{ke,\,PP}$=5.07, $N_{ke,\,TV}$=4.64, $N_{ke,\,LV}$=4.0, and $N_{ke,\,UU}$=3.11, respectively, which are much smaller than the N_{kt} values.

Similarly, laboratory obtained undrained shear strength values and CPTU tested "u_2-u_0" values are used as the X-axis and Y-axis values to calculate $N_{\Delta u}$. In Fig. 5, $N_{\Delta u,\,PP}$, $N_{\Delta u,\,LV}$, $N_{\Delta u,\,TV}$, and $N_{\Delta u,\,UU}$ represent the $N_{\Delta u}$ values for HBS overlying calcareous clay at Site W18-19 based on pocket penetrometer, torvane, miniature vane, and unconsolidated undrained triaxial tests, respectively. $N_{\Delta u}$ values obtained from Fig. 5 are $N_{\Delta u,\,PP}$=17.3, $N_{\Delta u,\,TV}$=16.3, $N_{\Delta u,\,LV}$=12.0, and $N_{\Delta u,\,UU}$=11.8, respectively, which are much larger than N_{ke} values but similar to N_{kt} values.

3.3 *Comparison of cone coefficients*

Cone coefficients based on different laboratory experiments and empirical models differ markedly. To determine further relationships among them, all obtained cone coefficients are listed in Table 2. Comparing the above results with those in Table 1, it is clear that cone coefficients for HBS overlying calcareous clayey silt in the Shenhu area are different to those reported in the literature, and the following inequality can be easily derived:

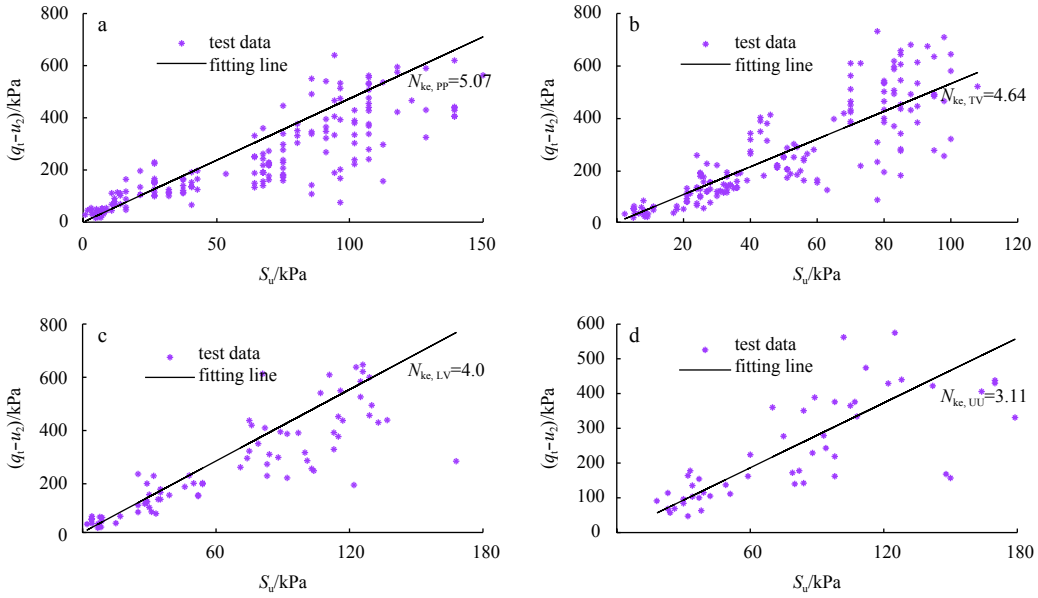

Fig. 4. Variations of q_t-u_2 versus the undrained shear strength determined by pocket penetrometer (a), torvane (b), miniature vane (c), and UU triaxial tests (d).

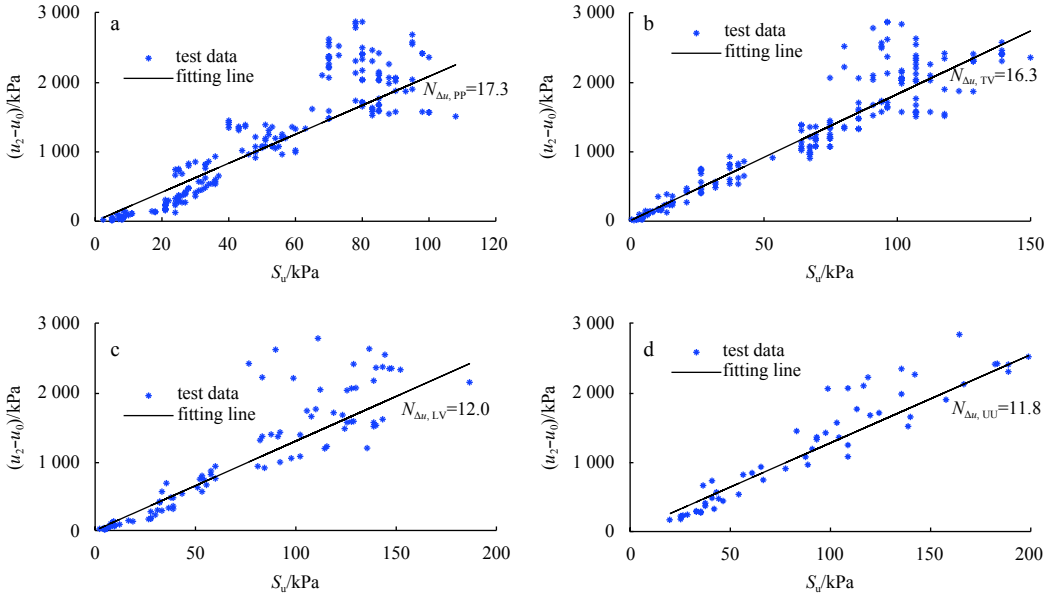

Fig. 5. Variations of u_2-u_0 versus the undrained shear strength determined by pocket penetrometer (a), torvane (b), miniature vane (c), and UU triaxial tests (d).

Table 2. Empirical cone coefficients for HBS overlying calcareous clay at Site W18-19 in the Shenhu area

Laboratory method	Excess-pore pressure model	Total cone resistance model	Effective cone resistance model
Pocket penetrometer	17.3	17.1	5.07
Torvane	16.3	15.2	4.64
Miniature vane	12.0	11.6	4.0
UU triaxial shear	11.8	11.1	3.11

$$N_{\mathrm{m,\,PP}} > N_{\mathrm{m,\,TV}} > N_{\mathrm{m,\,LV}} > N_{\mathrm{m,\,UU}}, \tag{6}$$

where subscript m equals ke, kt and Δu, which represent the excess-pore pressure model, the total cone resistance model, and the effective cone resistance model, respectively. By substituting Eq. (5) into empirical models expressed in Eqs (1)–(3), relative relationships among the undrained shear strength values calibrated using different laboratory experimental results can be written as Eq. (7):

$$S_{\mathrm{um,\,PP}} \leqslant S_{\mathrm{um,\,TV}} \leqslant S_{\mathrm{um,\,LV}} \leqslant S_{\mathrm{um,\,UU}}. \tag{7}$$

The above equations suggest that the undrained shear strength values calibrated by the pocket penetrometer test are relatively conservative. On the contrary, the undrained shear strength values calibrated by the unconsolidated undrained triaxial shear experiment are relatively extreme. For simple and precise prediction (i.e., not too conservative or too extreme), the average values of cone coefficients based on different laboratory experiments are used as the final cone coefficients for each empirical model, i.e.,

$$\left.\begin{aligned} N_{\Delta u} &= \text{average}\left\{N_{\Delta u,\,\mathrm{PP}}, N_{\Delta u,\,\mathrm{TV}}, N_{\Delta u,\,\mathrm{LV}}, N_{\Delta u,\,\mathrm{UU}}\right\} = 14.4 \\ N_{\mathrm{kt}} &= \text{average}\left\{N_{\mathrm{kt,\,PP}}, N_{\mathrm{kt,\,TV}}, N_{\mathrm{kt,\,LV}}, N_{\mathrm{kt,\,UU}}\right\} = 13.8 \\ N_{\mathrm{ke}} &= \text{average}\left\{N_{\mathrm{ke,\,PP}}, N_{\mathrm{ke,\,TV}}, N_{\mathrm{ke,\,LV}}, N_{\mathrm{ke,\,UU}}\right\} = 4.2 \end{aligned}\right\}. \tag{8}$$

Moreover, Table 2 suggests that the relative relationship between cone coefficients of the three empirical models can be expressed as in Eq. (9):

$$N_{\Delta u-\mathrm{n}} > N_{\mathrm{kt,\,n}} > N_{\mathrm{ke,\,n}}, \tag{9}$$

where subscript n equals PP, TV, LV and UU, which represent the pocket penetrometer, torvane, miniature vane, and unconsolidated undrained triaxial tests, respectively.

4 Model optimization and the undrained shear strength prediction for calcareous clay in the Shenhu area

4.1 *Optimized undrained shear strength prediction*

In case of no further detection, Eq. (8) is substituted into the undrained shear strength prediction models shown in Eqs (1) to (3). The vertical distribution of predicted undrained shear strength is shown in Fig. 6. The predicted results in Fig. 8 reflect the approximate distribution behaviors of the undrained shear strength for calcareous clayey strata in the Shenhu area. The variation in the curve predicted by the effective cone resistance model (Eq. (2)) is larger than the others, which may be because the effective cone resistance model contains both total cone resistance (q_t) and pore pressure (u_2), which were detected by the CPTU operation, but both the total cone resistance model (Eq. (1)) and excess-pore pressure model (Eq. (3)) involve only one CPTU para-

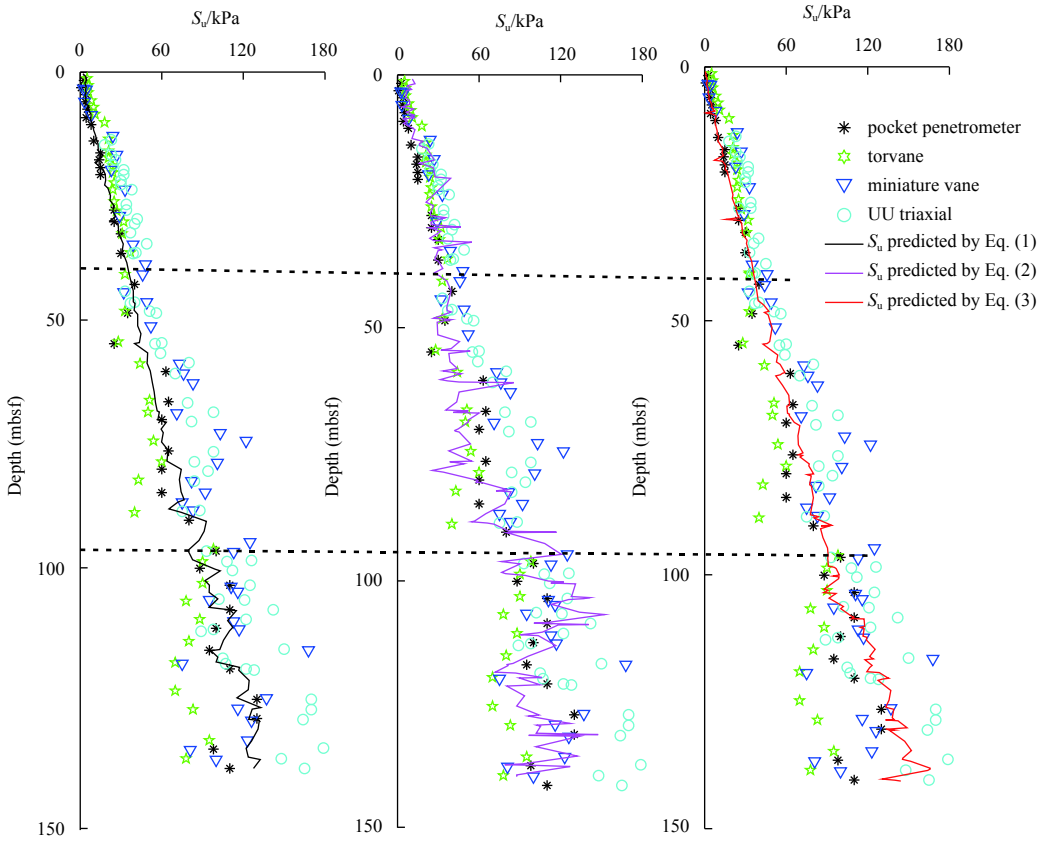

Fig. 6. Comparison between laboratory tests and model predicted results.

meter. This indicates that the effective cone resistance model (Eq. (2)) maybe more sensitive to CPTU results than the other two models. Accumulated measuring error from different CPTU parameters could cause vast fluctuations in the prediction results.

For more precise estimation of the undrained shear strength for calcareous clay in the study area, further observation is required to select and optimize the undrained shear strength prediction models for this area. The strata are divided into three intervals according to the fitting degrees between model prediction results and laboratory experimental results, as shown in Fig. 6. The effective cone resistance model (Eq. (2)) shows good adaptability for strata shallower than 38 mbsf, whereas prediction results from both the total cone resistance model (Eq. (1)) and excess-pore pressure model (Eq. (3)) are relatively conservative within 0–38 mbsf depth intervals. In the interval between 30 mbsf and 95 mbsf, prediction results based on Eq. (3) fit best with the laboratory results, while those based on Eq. (1) and Eq. (2) are smaller than average laboratory results. In intervals deeper than 95 mbsf, laboratory results tend to differ more from the prediction results. For a better description of the undrained shear strength within this depth interval, we choose the model whose results are closest to the average laboratory results as the optimal model; it is clear from Fig. 6 that the total cone resistance model (Eq. (1)) is the optimal model.

Generally, the best prediction models should vary with vertical depth, even for the same soil type (e.g., calcareous clay in this study). Optimized undrained shear strength prediction for calcareous clay in the Shenhu area can be written as in Eq. (10), in the format of a piecewise function.

$$S_{\mathrm{u}} = \begin{cases} \dfrac{q_{\mathrm{t}} - u_2}{N_{\mathrm{ke}}} & (H \leqslant 30\ \mathrm{mbsf}\,, N_{\mathrm{ke}} = 4.2)\,, \quad (10\mathrm{a}) \\ \dfrac{u_2 - u_0}{N_{\Delta u}} & (30\ \mathrm{mbsf} < H \leqslant 98\ \mathrm{mbsf}\,, N_{\Delta u} = 14.4)\,, \quad (10\mathrm{b}) \\ \dfrac{q_{\mathrm{t}} - \sigma_{\mathrm{v0}}}{N_{\mathrm{kt}}} & (H > 98\ \mathrm{mbsf}\,, N_{\mathrm{kt}} = 13.8)\,. \quad (10\mathrm{c}) \end{cases}$$

A comparison between laboratory results and model results predicted using Eq. (10) is shown in Fig. 7. The predicted results fit well with the laboratory results. This is very interesting because the adaptation boundaries of the optimized undrained shear strength prediction model coincide exactly with the boundaries of the soil layers. That is, very soft to firm clays are present from the mud-line to 30 mbsf, firm to very stiff but gasless clay layers are observed from 30.0 mbsf to 98.0 mbsf, and very stiff and gassy clays are dominant in intervals deeper than 98 mbsf. The soil layer classification and stiffness evaluation method will be discussed in future work and is not detailed here.

The first physical explanation of Eq. (10) involves the effects of gas. In the interval from 98 mbsf to the upper boundary of

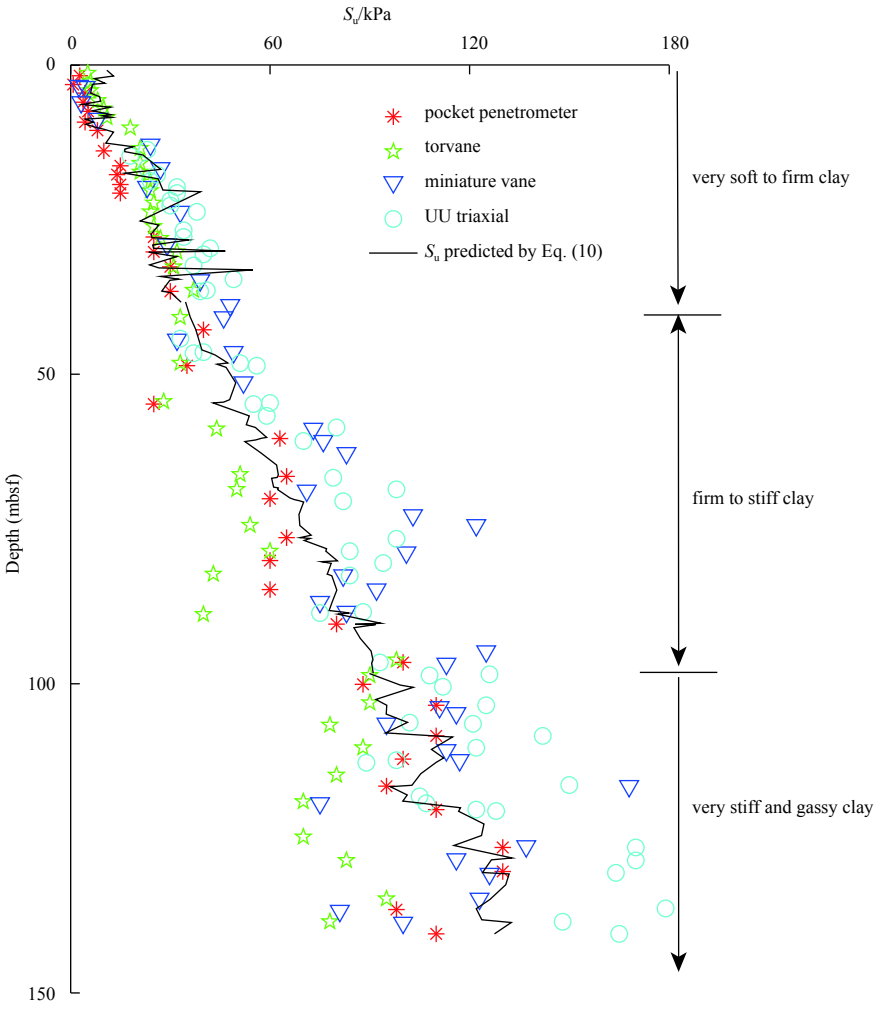

Fig. 7. Comparison between laboratory measurements and model results predicted using Eq. (10).

HBS, very stiff but gassy clays are observed. Gas compressibility may have a negative effect on pore pressure (u_2), which is measured by the water diffusion response (Cai et al., 2017; Sultan et al., 2010). Both Eq. (10a) and Eq. (10b) are related to the parameter u_2. Fluctuation of the curve obtained by Eq. (10a) and Eq. (10b) will increase with increased gas saturation. Therefore, Eq. (10c), which is independent of u_2, is most suitable for describing the undrained shear strength in intervals deeper than 98 mbsf. Secondly, differences between results predicted using Eq. (10a) and Eq. (10b) may be caused by the water saturation or compaction degree, but this mechanism should be comprehensively analyzed in further work.

The above phenomena indicate the adaptability of empirical models to calcareous clay soils in the Shenhu area. The effective cone resistance model is suitable for very soft to firm calcareous clays, the excess-pore pressure model can determine the undrained shear strength for firm to very stiff but gasless clays, and the total cone resistance model is more suitable for evaluating the undrained shear strength in very stiff and gassy clay soils.

4.2 *Model adaptability verification*

Normally, the statistical consistency of empirical model prediction results can be evaluated by three statistical criteria: the coefficient of determination (R^2), the root mean squared error (*RMSE*), and the mean absolute error (*MAE*).The higher the R^2, the greater the adaptability of the optimized model. However, lower values of *RMSE* and *MAE* lead to a smaller dispersion of predicted values and better accuracy of the optimized results. Therefore, the statistical criteria for adaptability of the optimized model can be defined as:

$$R^2 = 1 - \frac{\sum_{i=1}^{n} \left(S_{\mathrm{u,lab}} - S_{\mathrm{u,pre}}\right)^2}{\sum_{i=1}^{n} \left(S_{\mathrm{u,lab}} - \bar{S}_{\mathrm{u,lab}}\right)^2}, \tag{11}$$

$$RMSE = \sqrt{\frac{\sum_{i=1}^{n} \left(S_{\mathrm{u,lab}} - S_{\mathrm{u,pre}}\right)^2}{n}}, \tag{12}$$

$$MAE = \frac{\sum_{i=1}^{n} \left|S_{\mathrm{u,lab}} - S_{\mathrm{u,pre}}\right|}{n}, \tag{13}$$

where $S_{\mathrm{u,\,lab}}$ and $S_{\mathrm{u,\,pre}}$ are the laboratory measured undrained shear strength and model predicted values by Eq. (10), respectively; $\bar{S}_{\mathrm{u,\,pre}}$ is the average of the laboratory measured values; and n represents the number of data points.

The relationship between models predicted undrained shear strength values and laboratory measured values is shown in Fig. 8. In this figure, the closer the scattered points to the 45° line, the better the fitting degree. The area defined by 60% and 160% of the 45° line can be defined as the acceptable deviation area. We conclude from Fig. 8b that 8.5% (approximately 40 points) of scattered points lie in the upper left region of the acceptable deviation area, which indicates that results predicted by the effective cone resistance model (Eq. (2)) tend to be slightly conservative. This is especially true for very stiff and gassy strata, as shown in Fig. 6. On the other hand, for the results predicted by the excess-pore pressure model, approximately 8% of scattered points lie in the area below the right region of the acceptable deviation area

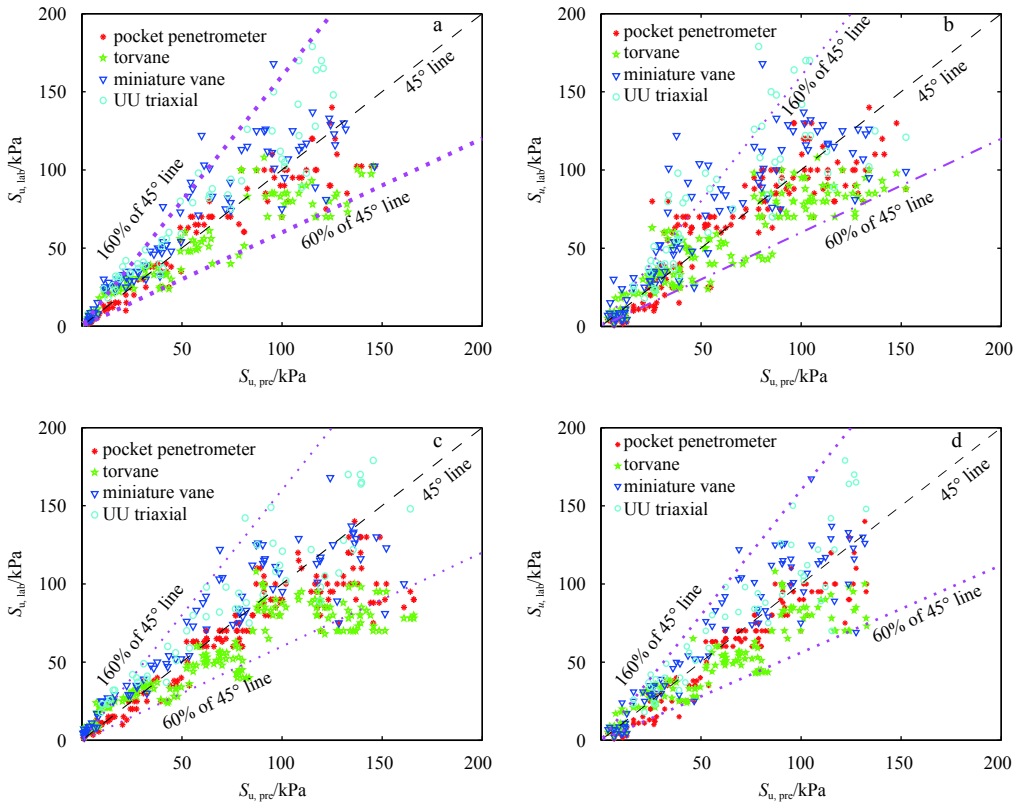

Fig. 8. Relationship between laboratory measured undrained shear strength and model predicted values by the total cone resistance model (a), the effective cone resistance model (b), the excess-pore pressure model (c), and the optimized model in pricewise function format (d).

(60% of the 45° line). For Figs 8a and d, deviation of data points from the 45° line is limited (97% of points lie in the acceptable deviation area). For more comparison, the statistical criteria values for different models are summarized in Table 3. It is clear that the optimized model considerably improves the adaptability of empirical models for calcareous clay in the Shenhu area of the northern South China Sea.

Table 3. Comparison of statistical criteria values

Model	R^2	*RMSE*/kPa	*MAE*/kPa
Total cone resistance model	0.75	19.4	13.3
Effective cone resistance model	0.63	23.1	16.5
Excess-pore pressure model	0.56	25.4	17.4
Optimized piecewise function model	0.80	16.8	12.1

5 Conclusions

(1) The HBS overlying strata at Site W18-19 in the Shenhu area of the northern South China Sea mainly consists of calcareous clays. The undrained shear strength increases with depth. Mathematical and statistical analysis reveals that the cone coefficients based on different laboratory experiments and prediction models show significant variation. The following two relationships are always valid: $N_{m,\,PP}>N_{m,\,TV}>N_{m,\,LV}>N_{m,\,UU}$ and $N_{\Delta u,\,n}>N_{kt,\,n}>N_{ke,\,n}$.

(2) The adaptation boundaries of the empirical prediction models coincide exactly with the soil layer boundaries. The effective cone resistance model is suitable for very soft to firm calcareous clays, the excess-pore pressure model can depict undrained shear strength for firm to very stiff but gasless clays, and the total cone resistance model is better at evaluating the undrained shear strength for very stiff and gassy clays.

(3) The optimized model in piecewise function format can depict the longitudinal distribution of the undrained shear strength in overlying the HBS strata in the study area, with statistical criteria values of R^2=0.80, the *RMSE* being 16.8 kPa, and the *MAE* being 12.1 kPa.

References

Aas G, Lacasse S, Lunne T, et al. 1986. Use of In Situ Tests in Geotechnical Engineering. American Society of Civil Engineers, New York, NY: 1–15

An Yanyong, Guo Yanmo, Li Xiangfeng. 2009. Analysis of pore pressure static cone penetration test to determine soft clay strength. Site Investigation Science and Technology (in Chinese), (3): 8–12

Cai Guojun, Lin Jun, Liu Songyu, et al. 2017. Characterization of spatial variability of CPTU data in a liquefaction site improved by vibro-compaction method. KSCE Journal of Civil Engineering, 21(1): 209–219, doi: 10.1007/s12205-016-0631-1

Cai Guojun, Liu Songyu, Puppala A J. 2016. Evaluation of geotechnical parameters of a lagoonal clay deposit in Jiangsu Lixia River area of China by seismic piezocone tests. KSCE Journal of Civil Engineering, 20(5): 1769–1782, doi: 10.1007/s12205-015-0164-z

Ching J, Phoon K K. 2012. Modeling parameters of structured clays as a multivariate normal distribution. Canadian Geotechnical Journal, 49(5): 522–545, doi: 10.1139/t2012-015

Chung S F, Randolph M F, Schneider J A. 2006. Effect of penetration rate on penetrometer resistance in clay. Journal of Geotechnical and Geoenvironmental Engineering, 132(9): 1188–1196, doi: 10.1061/(ASCE)1090-0241(2006)132:9(1188)

Ebrahimian B, Movahed V, Pasha A Y. 2012. Evaluation of undrained shear strength of marine clay using cone penetration resistance at South Pars field in Iran. Ocean Engineering, 54: 182–195, doi: 10.1016/j.oceaneng.2012.07.018

Han Hongwei, Li Zhijun, Huang Wenfeng, et al. 2015. The uniaxial compressive strength of the arctic summer sea ice. Acta Oceanologica Sinica, 34(1): 129–136, doi: 10.1007/s13131-015-0598-7

Hu Gaowei, Li Yanlong, Wu Nengyou, et al. 2017. Undrained shear strength estimation of the cover layer of hydrate at Site W18/19 of Shenhu area. Marine Geology & Quaternary Geology (in Chinese), 37(5): 151–158

Ji Fudong, Jia Yonggang, Liu Xiaolei, et al. 2016. In situ measurement of the engineering mechanical properties of seafloor sediment. Marine Geology & Quaternary Geology (in Chinese), 36(3): 191–200

Konrad J M, Law K T. 2015. Preconsolidation pressure from piezocone tests in marine clays. Géotechnique, 37(2): 177–190

Kvenvolden K A. 1998. A primer on the geological occurrence of gas hydrate. Geological Society London Special Publications, 137(1): 9–30, doi: 10.1144/GSL.SP.1998.137.01.02

La R, Zebdi M, Leroueil S, et al. 1990. Piezocone tests in sensitive clays of eastern Canada. International Journal of Rock Mechanics & Mining Sciences & Geomechanics Abstracts, 27(6): 353–356

Li Yanlong, Liu Changling, Liu Lele. 2016a. Damage statistic constitutive model of hydrate-bearing sediments and the determination method of parameters. Acta Petrolei Sinica (in Chinese), 37(10): 1273–1279

Li Yanlong, Liu Changling, Liu Lele, et al. 2016b. Key issues for triaxial test of hydrate-bearing sediment. Advances in New and Renewable Energy (in Chinese), 4(4): 279–285

Li Xuepeng, Yang Xiaojuan, Cai Guojun, et al. 2016. Determination of undrained shear strength of clayey soil in Ningbo based on CPTU. Journal of Chongqing Jiaotong University (in Chinese), 35(6): 20–23, 50

Liu Changling, Meng Qingguo, Hu Gaowei, et al. 2017. Characterization of hydrate-bearing sediments recovered from the Shenhu area of the South China Sea. Interpretation, 5(3): SM13–SM23, doi: 10.1190/INT-2016-0211.1

Liu Weizheng, Shi Minglei, Xu Linrong. 2013. Elastoplastic analysis of cylindrical cavity expansion in natural sedimentary soft clay with structure damage. Chinese Journal of Geotechnical Engineering (in Chinese), 35(3): 487–494

Low H E, Randolph M F. 2010. Strength measurement for near-seabed surface soft soil using manually operated miniature full-flow penetrometer. Journal of Geotechnical and Geoenvironmental Engineering, 136(11): 1565–1573, doi: 10.1061/(ASCE)GT.1943-5606.0000379

Lunne T, Christoffersen H, Tjelta, et al. 1987. Engineering use of piezocone data in North Sea clays. International Journal of Rock Mechanics & Mining Sciences & Geo-mechanics Abstracts, 24: 92

Ma Haopeng, Chen Zuyu, Yu Shu. 2014. Correlations of soil shear strength with specific penetration resistance of CPT in Shanghai area. Rock and Soil Mechanics (in Chinese), 35(2): 536–542

Młynarek Z, Gogolik S, Półtorak J. 2012. The effect of varied stiffness of soil layers on interpretation of CPTU penetration characteristics. Archives of Civil and Mechanical Engineering, 12(2): 253–264, doi: 10.1016/j.acme.2012.03.013

Senneset K, Janbu N, Svano G. 1982. Strength and deformation parameters for CPT. In: Proceedings of the 2nd European Symposium on Penetration Testing. Amsterdam, The Netherlands

Shin Y J, Kim D. 2011. Assessment of undrained shear strength based on cone penetration test (CPT) for clayey soils. KSCE Journal of Civil Engineering, 15(7): 1161–1166, doi: 10.1007/s12205-011-0808-6

Sultan N, Savoye B, Jouet G, et al. 2010. Investigation of a possible submarine landslide at the Var delta front (Nice continental slope, southeast France). Canadian Geotechnical Journal, 47(4): 486–496, doi: 10.1139/T09-105

Tong Liyuan, Wang Qiang, Du Guangyin, et al. 2011. Determination of undrained shear strength using piezocone penetration test in clayey soil for bridge foundation. Journal of Southeast University, 27(2): 201–205

Wang Yanmin, Liu Shaowen, Hao Feifei, et al. 2017. Geothermal investigation of the thickness of gas hydrate stability zone in the

north continental margin of the South China Sea. Acta Oceanologica Sinica, 36(4): 72–79, doi: 10.1007/s13131-017-1014-2

Wei L, Pant R, Tumay M T. 2010. Evaluation of undrained shear strength of soft New Orleans clay using piezocone. In: Proceedings of the 2nd International Symposium on Cone Penetration Testing. Huntington Beach, CA

Wu Nengyou, Yang Shengxiong, Zhang Haiqi, et al. 2010. Gas hydrate system of Shenhu Area, northern South China Sea: wireline logging, geochemical results and preliminary resources estimates. In: Offshore Technology Conference. Houston, Texas, USA

Wu Nengyou, Zhang Haiqi, Yang Shengxiong, et al. 2011. Gas hydrate system of Shenhu area, northern South China Sea: Geochemical Results. Journal of Geological Research, 2011: 370298

Yang Yijun, Tong Liyuan, Zhu Ning, et al. 2016. Evaluation and application of undrained shear strength in excavation from piezocone tests (CPTU). Chinese Journal of Underground Space and Engineering (in Chinese), 12(4): 1095–1101

Yang Shengxiong, Zhang Ming, Liang Jinqiang, et al. 2015. Preliminary results of China's third gas hydrate drilling expedition: a critical step from discovery to development in the South China Sea. Fire in the Ice, 15(2): 1–5